IEEE Access
Multidisciplinary ⋮ Rapid Review ⋮ Open Access Journal

Received September 19, 2020, accepted September 29, 2020, date of publication October 1, 2020, date of current version October 14, 2020.

Digital Object Identifier 10.1109/ACCESS.2020.3028283

Increase in Volumetric Electrical Power Density of a Linear Generator by Winding Optimization for Wave Energy Extraction

SELIM MOLLA[1], (Member, IEEE), OMAR FARROK[1], (Member, IEEE), ABIDUR RAHMAN[1], MD. SAMIUL BASHIR[1], MD. RABIUL ISLAM[2], (Senior Member, IEEE), ABBAS Z. KOUZANI[3], (Member, IEEE), AND M. A. PARVEZ MAHMUD[3]

[1]Department of Electrical and Electronic Engineering, Ahsanullah University of Science and Technology, Dhaka 1208, Bangladesh
[2]School of Electrical Computer and Telecommunications Engineering, University of Wollongong, Wollongong, NSW 2522, Australia
[3]School of Engineering, Deakin University, Geelong, VIC 3216, Australia

Corresponding author: Omar Farrok (omarruet@gmail.com)

ABSTRACT In this article, a method of winding optimization of the linear generator is proposed to increase the electrical power generation from the oceanic wave. A linear generator is designed in the ANSYS/Maxwell environment to analyze the proposed winding optimization method. The electrical and magnetic properties of the generator are extensively analyzed. The cross-sectional area and the number of turns of the copper conductor are optimized to maximize the output power. Load characteristics are also considered for different conductor sizes and turn numbers to determine a suitable operating point. A cooling system is also incorporated in the optimized linear generator to extract the thermal energy produced during the operation, which eventually enhances the electrical power generation. It is found that the optimized linear generator finally generates around 42% more electrical power compared to that of the conventional one. Therefore, the volumetric power density of the linear generator is noticeably increased with the proposed optimization method that also results in the minimization of material cost of the generator. A downscale prototype of the linear generator is constructed in the laboratory. It is expected that the proposed winding optimization method can be used in designing other linear generators.

INDEX TERMS Cooling system, electrical generator, energy conversion, linear generator, magnetic material, permanent magnet machine, power density, wave energy converter, wave power, winding optimization.

I. INTRODUCTION

To ensure sustainable environment, the United Nations has declared seventeen sustainable development goals in which affordable and clean energy is positioned at number seven. Still, significant amount of electrical power is being generated from fossil fuels. This burning of fossil fuels is highly affecting the environment due to the huge emission of carbon di oxide (CO_2). Emission of CO_2 is highly affecting the global temperature. The increase in temperature causes melting of glacier ice that continuously raises the sea level. It also increases conflagration in many dry regions and the quality of habitual land is debasing rapidly. On the other hand, burning of huge fossil fuel diminishes the reserve of the natural resources. Considering the environmental degradation and depletion of natural resources, alternative sources of energy, i.e. renewable energy is becoming one of the main sources of energy in many countries [1].

Solar, wind, biogas, hydro, geothermal, and oceanic wave energy are remarkable examples of renewable energy sources. Some of these sources are intermittent in nature such as wind and solar. As a result, production and use of electricity from these intermittent sources require some extra devices and investments [2], [3]. The costly energy storage systems with periodic maintenance are often required for their smooth operation. Hydropower and geothermal energy sources are available only in a few specific locations [4], [5]. On the other hand, oceanic wave is an attractive renewable energy source which does not have the limitation of availability compared to solar and wind energy. In addition, oceanic wave energy

The associate editor coordinating the review of this manuscript and approving it for publication was Jinquan Xu.

has some other features such as its high energy density and predictability [6]. It is found that, approximately 1–10TW electric power can be extracted from the ocean [7]. The wave power, P_w can be calculated from

$$P_w = \frac{\rho_w}{64\pi} g^2 H_w^2 T \tag{1}$$

where ρ_w is the mass density of sea water (1025 kg/m^3), H_w is the height of wave, g is the gravitational constant (9.81 ms^{-2}), and T is the time period of wave [8]. Although, the idea of capturing oceanic wave energy was introduced in 1799 as reported in [9], but the major development was started from 1973 due to oil crisis [10]. Different types of devices are applied to harvest oceanic wave energy such as Pelamis, Wave Dragon, Limpet etc. In most of the cases, direct drive linear generator (DDLG) topology is incorporated, which is illustrated in Fig. 1.

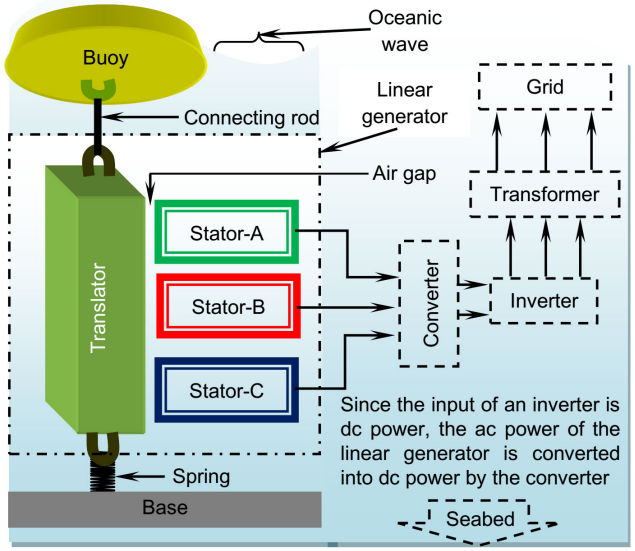

FIGURE 1. Sea wave energy conversion system.

The wave energy converter has mainly five parts viz. buoy, DDLG, converter, inverter, and transformer. The DDLG is generally a three-phase linear electrical generator that consists of a translator and a stator set with three windings. Upper side of the translator is connected with a buoy by a rod. The other side is connected to the base with a spring. When the buoy moves vertically with the sea wave, translator moves along with the buoy. As a result, electromotive force is induced in the stator windings. The generated ac power has variable voltage and frequency. Therefore, it is rectified and fed to the inverter to obtain fixed voltage and frequency. Then the ac power is supplied to the load or grid through the transformer.

At present, linear generators (LGs) are being characterized through mathematical, simulation, and/or experimental approach. A new cycloidal type wave energy converter is explained with numerical simulation to estimate the power absorption annually [11]. A novel dual port LG is proposed in [12], which can generate electrical power even at zero vertical velocity of the buoy with the aid of a driven translator. To ensure the maximum absorption of sea wave energy, a smart controller is designed in [13]. In [14], transient stability of a grid connected wave energy converter is obtained using a proportional-integral controller which is designed with water cycle algorithm. Another study incorporates gravitational search algorithm to control wave energy converter under various operating conditions [15]. The winding of a tubular LG is prepared with the superconductor to obtain high output power [16]. However, a cooling system is required for maintaining cryogenic temperature of the superconductor, which is a challenging task.

The amount of produced thermal energy inside the LG is proportional to the losses: viz. mechanical loss, core loss, and copper loss. On the other hand, the demagnetization effect of permanent magnet (PM) depends on temperature. Hence, the output power of permanent magnet based DDLG depends on its operating temperature. Most of the DDLG are made of conventional PM, which cannot generate enough output power because of their early demagnetization. To solve this problem, the high grade neodymium iron boron (NdFeB) PM, N52 is applied to the LG that delivers more output power than the conventional one [17]. Since neodymium is a rare earth element, the LG is designed with a new rare earth free material named iron nitride ($Fe_{16}N_2$) instead of NdFeB [18]. Core loss of an LG is reduced in [19] by applying DI-Max HF-10X magnetic core because, it enables generating more output power compared to its conventional counterpart. The magnetic circuit of an ordinary LG is asymmetric which results in some shortcomings that impede its performance [20].

It is found from the analysis that, winding optimization significantly increases the electrical power generation of the LG. But, to the best of authors' knowledge, copper-based winding optimization is still not investigated for power enhancement. Therefore, there is a research gap regarding the winding optimization method which is needful for the enhancement of power generation. For this reason, a novel winding optimization method is proposed in this article that greatly increases the electrical power generation of the LG. The proposed method would enhance the knowledge in this area for the future development of LG. The novelty of this article is summarized as follows:

- A novel winding optimization algorithm is proposed for the DDLG to increase the power generation.
- The proposed winding optimization algorithm is applied to the generator to observe its effectiveness.
- The effect of using an advanced permanent magnet (N45) in the generator is analyzed.
- The cooling system for maintaining magnetic properties of the high graded material is incorporated for further enhancement of the electrical power generation of the generator.
- The volumetric power density of the generator is increased.

This article comprises seven sections. The proposed optimization method is discussed in section II. Construction of

the proposed linear generator is described in section III. Mathematical models of the DDLG and cooling system are presented in section IV. The procedure of cooling method is depicted in section V. Results are provided in section VI. The consequent section concludes the paper.

II. THE PROPOSED WINDING OPTIMIZATION

Winding optimization of the LG is important to minimize the size and weight and to enhance the energy conversion efficiency. In [21], the shape of an LG is optimized for minimizing the volume of steel core in translator and stator by applying the human intervened genetic algorithm. Two-dimensional geometry is considered for the analysis by finite element method. Approximately, 29% more power is measured with the 'M' shaped core and copper winding.

The structure of an LG is optimized in [22] to achieve better output voltage and reduced cogging force. The system consists of four translators connected together with a buoy. Magnetic characteristics of the generator are analyzed with the aid of two-dimensional finite element analysis. The generator is further analyzed by using a numerical method. In [23], historical wave data are collected to maximize the voltage and output power. A bang-bang type control mechanism is applied to wave energy converter in [24] for obtaining optimum output power.

Genetic algorithm is applied in [25] to optimize the shape of an LG to achieve maximum output power while minimizing the weight of the translator. In addition, the reduction of core loss and generation of large output power are achieved by applying appropriate magnetic materials [17]–[19]. In addition, the output power is enhanced by applying high graded magnetic materials namely DI-Max HF-10 core, Supermendur core, N52 PM, and iron nitride PM.

Although, the optimization of linear generator is discussed in [12], [23]–[26] with different objectives, winding optimization is not yet investigated. In order to fill the knowledge gap, a method of winding optimization of the linear generator is proposed in this article to increase the electrical power generation from the oceanic wave. Various factors such as mesh setup, boundary conditions, construction, insulating, and active materials are considered. Performance of the LG is observed by analysis through induced voltage, load current, flux linkage, and output power. The simulation continues iteratively until satisfactory results are found. Fig. 2 illustrates the flowchart of the proposed winding optimization method.

Copper loss occurs due to winding resistance that further minimizes output power of the linear generator. Hence, low winding resistance would produce low copper loss. On the other hand, the induced voltage is directly proportional to the number of turns that results in high winding resistance. Hence, the proposed winding optimization solves the dilemma by which suitable turn number and conductor size for maximum power generation are determined. Load characteristics are analyzed to find the operating point for the highest output power.

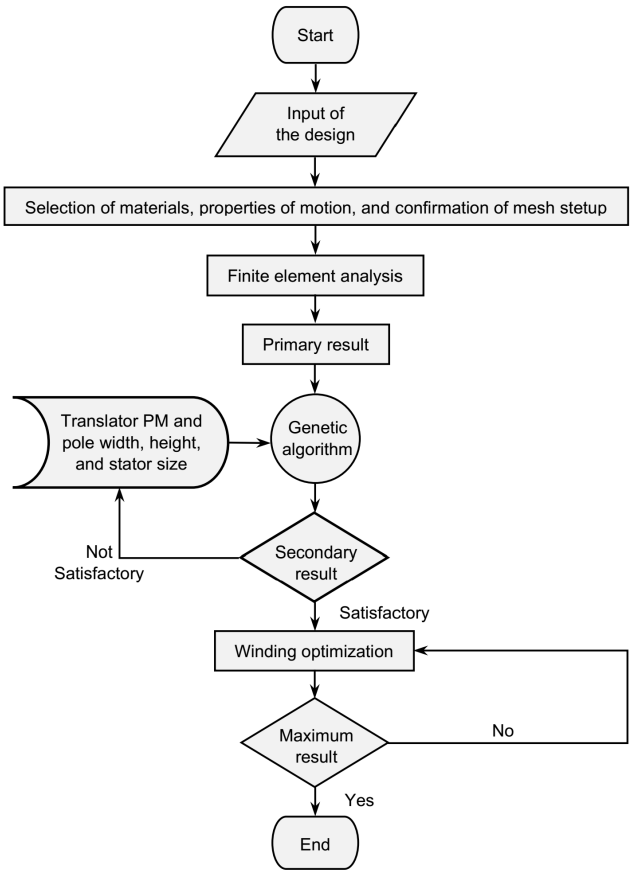

FIGURE 2. Procedure of the proposed optimization.

Initially, the whole linear generator is constructed using its geometrical data. Afterwards, the properties of materials for the translator, core, permanent magnet, coil etc. are selected and applied to the simulation setup. Consequently, the motion properties are defined along with mesh setup. After that, the finite element analysis is conducted for the proposed design of the linear generator. The primary result found from the analysis is evaluated until the dimensions of the linear generator are optimized. Afterwards, winding optimization is conducted for better output. The output power is further increased with the application of a cooling system and high graded magnetic material.

III. CONSTRUCTION OF THE LINEAR GENERATOR

The proposed generator has mainly two parts, i.e. stator and translator. The translator consists of the magnetic core and PM. On the contrary, each of the stator has a magnetic core and copper winding. Construction of the DDLG and properties of magnetic materials are described in the following subsections. The generated voltage is directly proportional to the turn number of winding, which can be calculated as

$$e = -N\frac{d\phi}{dt} \tag{2}$$

where e is the induced voltage in the stator, N is the turn number, φ is the magnetic flux, and t is the time.

A. CONSTRUCTION

The stator is made of "E" type ferromagnetic material where different conductor sizes are applied for winding optimization. The design is illustrated in Fig. 3 with a prototype. The conductor sizes are considered 5mm^2, 4mm^2, 3mm^2, and 2mm^2 as denoted by X-5, X-4, X-3, and X-2, respectively. The conductor, X-3 is selected in the experimental prototype as shown in Fig. 3(b). Geometry and construction of the proposed three phase LG are presented in Table 1 and Fig. 4, respectively. The "E" shaped magnetic core is shown separately. The conductor coil is placed in the middle of the core forming the stator of phase-A. Other two phases, i.e. phase-B and phase-C are constructed similarly. The stator and translator are placed vertically maintaining air gap.

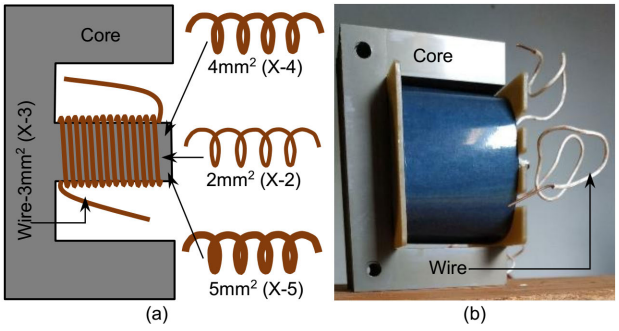

FIGURE 3. Construction of the stator: (a) CAD drawing and (b) the prototype.

TABLE 1. Geometry of the proposed LG.

Name of Parameters	Magnitude
Height of translator, H_t (m)	4.34
Length of translator, L_t (m)	2.4
Width of translator, W_t (m)	2
Core's thickness of translator, t_c (m)	0.022
Core's length of translator, L_c (m)	2.4
PM's thickness of translator, t_m (m)	0.038
PM's length of translator, L_m (m)	2.4
PM's width of translator, W_m (m)	1.99
Height of stator, H_s (m)	0.142
Winding's length of stator, L_s (m)	2.7
Winding's width of stator, W_s (m)	0.25

The translator is constructed with permanent magnet and magnetic cores. Both faces of a magnetic core are coupled with the permanent magnet following proper orientation. Windings are wounded separately on the magnetic core. Space inside the "E" core allocates total 918mm^2 cross-sectional area of the coil, which determines N as well. Winding with thin wire requires more turns than that of the large cross-sectional wire. Moreover, thin and long conductors result in high resistance which can be calculated as

$$R = \rho \frac{L}{A} \tag{3}$$

where R is the resistance, ρ is the resistivity, L is the length of copper wire, and A is the cross-sectional area of the conductor. Thus, with a total 918mm^2 cross-sectional space in the stator, the possible maximum number of turns are 460, 306, 230, and 184 for X-2, X-3, X-4, and X-5 wires, respectively. Phasor diagram of the proposed LG is shown in Fig. 5.

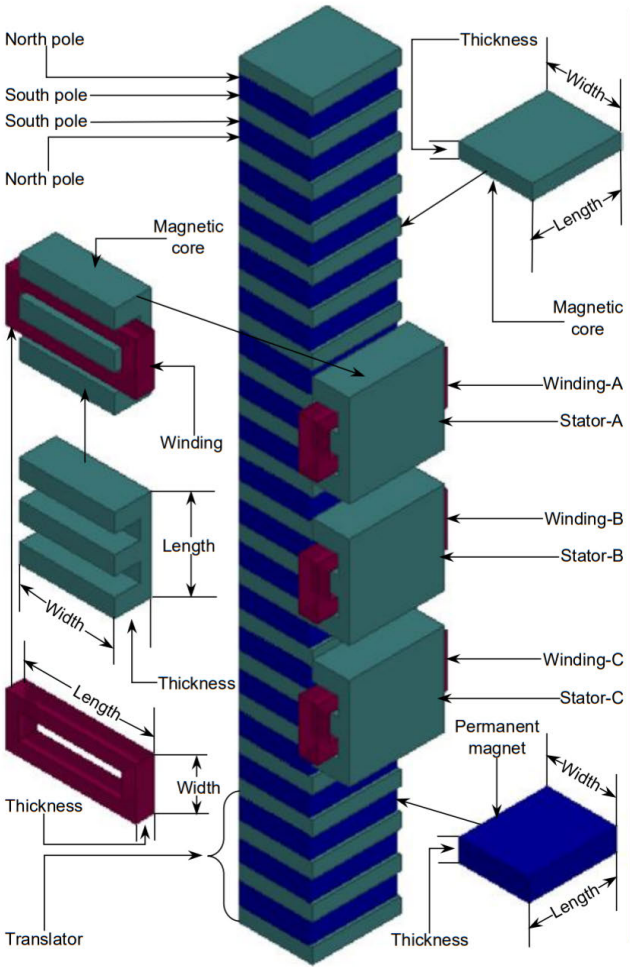

FIGURE 4. Basic construction of the proposed DDLG.

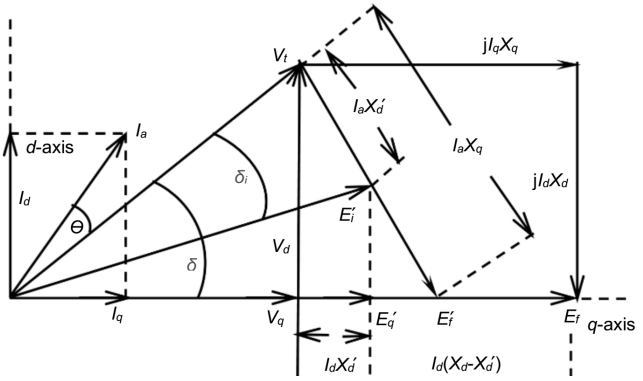

FIGURE 5. Phasor diagram of the proposed DDLG.

B. PROPERTIES OF MAGNETIC MATERIALS

Demagnetizing curves for both the conventional N30H and high graded N45 permanent magnets are shown in Fig. 6.

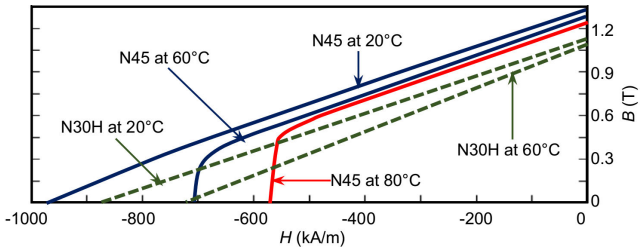

FIGURE 6. Demagnetizing curves of the conventional N30H and high graded N45 permanent magnets.

TABLE 2. Comparison of magnetic properties between two materials.

Output parameters	N30H NdFeB	N45 NdFeB
Remanence magnetism (T)	1.1	1.37
Coercivity (A/m)	−837999.99	−965000
Relative permeability	1.0446	1.173
Bulk conductivity (S/m)	625000	625300
Mass density (Kg/m^3)	7550	7550

IV. MATHEMATICAL MODEL OF THE PROPOSED SYSTEM

The proposed system consists of two sections. One is the DDLG itself and the other is cooling system. The proposed linear generator is described mathematically in the following sub-section. The losses that occur are also formulated. The proposed cooling system is demonstrated in the successive sub-section.

A. MODEL FOR THE PROPOSED DDLG

In this section, voltage, current, power, core loss and copper loss of the proposed LG are described mathematically using two axis model. The stator voltage of the proposed machine can be computed as

$$\bar{S}_a = \frac{f_{do} + jf_{qo}}{\sqrt{3}}; \quad \bar{V}_t = r_a\bar{I}_a + X_q\bar{I}_q + jX_dI_d + jE_F \tag{4}$$

where S_a is the stator voltage, r_a is the resistance of stator winding, I_a is the stator current, I_q is the current in quadrature axis (q-axis), I_d is the current in direct axis (d-axis), X_q is the reactance of q-axis, E_F is the voltage of equivalent field, X_d is the reactance of d-axis, f_{do} is the voltage of d-axis without damper, and f_{qo} is the voltage in q-axis without damper. Since the proposed DDLG is a synchronous machine, E_F must be ahead of V_t. The output power, P_0 can be calculated as

$$P_0 = \frac{V_tE_F}{X_d}sin\delta + \frac{V_t^2}{2}\left(\frac{1}{X_q} - \frac{1}{X_d}\right)sin2\delta \tag{5}$$

where δ is the torque angle. The core loss of the proposed machine is calculated from

$$P_c = P_e + P_h + P_{ad} \tag{6}$$

where P_c is the total core loss, P_e is the eddy current loss, P_h is the hysteresis loss, and P_{ad} is the excess loss. The generalized expression (7) can be used to calculate the core loss.

$$P_c = M_ef^2B_m^c \tag{7}$$

where f is the voltage frequency, B_m is the maximum flux density, c is the constant that depends on properties of the magnetic material, M_e is the core loss components. Copper loss can be calculated as

$$P_{Cu} = I_a^2r_a \tag{8}$$

B. COOLING SYSTEM MODEL

To control the cooling process, a mathematical model is developed in [26] which is adopted in this article so that the variables for heat reducing method can be calculated. The amount of water that is lost due to evaporation can be assessed by observing the states of air passing through a cooling tower. The block diagram describing the procedure of the proposed cooling system is depicted in Fig. 7.

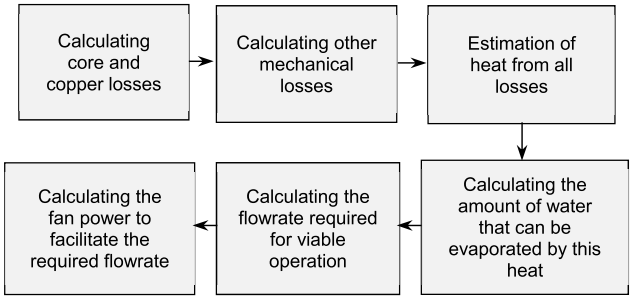

FIGURE 7. Functional block diagram of the proposed chiller.

The first step is to calculate the core and copper losses. After that, the mechanical losses due to friction, inertia etc. are considered. Afterwards, the amount of heat that is generated from the loss is estimated.

Dissipation of heat energy is performed by water evaporation. Thus, the amount of water required to absorb the estimated heat is calculated. Subsequently, flowrates of water and air for viable operation are determined.

The rate of evaporated water loss is expressed with the difference between mass flowrate of water entering the tower, m_{te} and mass flowrate of water leaving the tower, m_{tl}. It can also be determined by multiplying mass flowrate of air, m_a with the difference between the moisture content of air leaving the tower, ω_{tl} and moisture content of air entering the tower, ω_{te}. The value of m_a can be computed as

$$m_{te} - m_{tl} = m_a\left(\omega_{tl} - \omega_{te}\right). \tag{9}$$

The relationship between fan power, P and m_a can be expressed as

$$P = P_r\left(\frac{m_a}{m_{ar}}\right)^n \tag{10}$$

where m_{ar} is the nominal mass flowrate of air entering the cooling tower and P_r is the rated power of the fan. The value of n is 1 for the constant fan speed. If the fan is operated at variable speed, the value of n becomes 3 according to cube law. The cooling system for the proposed DDLG incorporates variable speed drive to operate the fan at any speed.

The consumed power of the fan is considered 3% of the total power. The minimum flowrate is approximately 10% of the rated flowrate. Hence, if the temperature range is known, fan power can be computed easily.

V. COOLING SYSTEM FOR LINEAR GENERATOR

Any permanent magnet LG works properly under low temperature. With the rise of temperature because of core and copper losses, performance of the LG degrades considerably. Therefore, a cooling system is installed to reduce the temperature of the LG so that the magnetic properties do not get deteriorated. The proposed cooling system is described as follows.

A. COOLING SYSTEM CONSTRUCTION

The complete cooling system for the proposed LG comprises a chiller, control panel, dehumidifier, supply chilled water pipe (SCWP), return chilled water pipe (RCWP), and air management unit (AMU) with dehumidifier (DHF) as illustrated in Fig. 8.

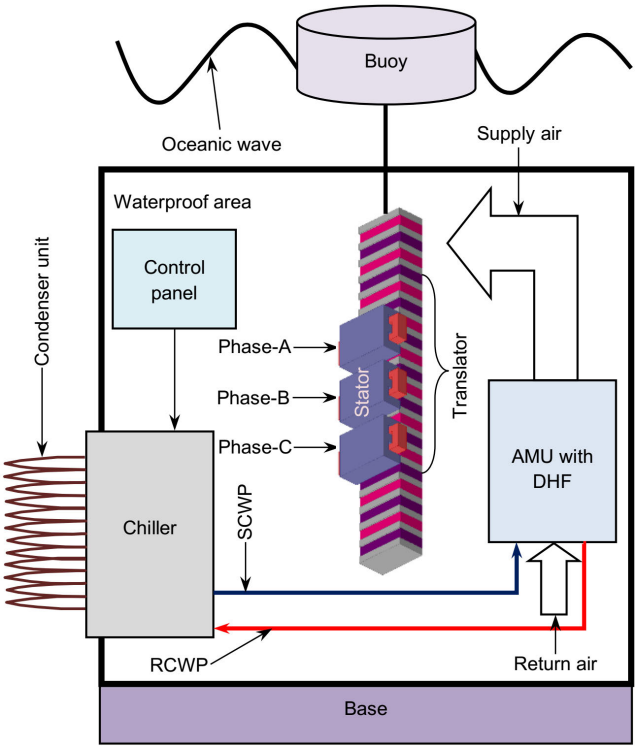

FIGURE 8. Cooling system for the proposed DDLG.

To monitor and control the functionality of the cooling system, three different sensors are placed at different locations. One sensor is placed on RCWP to measure the temperature of chilled water. Other two sensors monitor the humidity and temperature of the proposed DDLG. The data from the sensors are sent to control panel which operates the dehumidifier, AMU, and the chiller to maintain the humidity and temperature.

The chiller is an electromechanical device which can noticeably decrease the temperature of water. The underlying components of this device are evaporator, condenser, compressor, expansion valve, solenoid valve, and filter core as shown in Fig. 9.

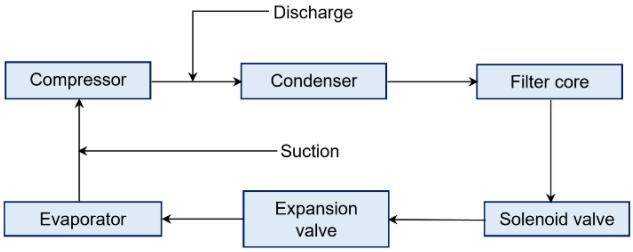

FIGURE 9. Block diagram of the chiller unit.

The control panel maintains the whole process in accordance with the signal of the sensors. The chiller unit is filled with R410a refrigerant. At relaxation mode, suction pressure is maintained at 80PSI whereas at functioning mode, the pressure is reduced and kept at 50–65PSI. In contrast, the discharge pressure at functioning mode is kept at approximately 250PSI. The pressure at relaxation mode is the same for both suction and discharge pressure. After starting the compressor, the pressure of R410a refrigerant rises from 80PSI to 250PSI. Afterwards, it is passed on to the condenser unit. The condenser unit is made of aluminum fins and copper coil. By this time, the temperature on discharge tube increases to 70–80°C. The refrigerant, upon entering the chiller unit, releases its pressure and temperature which changes its state from gas to liquid. Afterwards, it moves through the filter core where the flow is controlled by the solenoid valve. This valve is regulated by the control panel and delivers the refrigerant to the expansion valve. Depending on the signal of a gas operated valve sensor, the refrigerant again changes its state from liquid to vapor inside the expansion valve chamber. Then refrigerant flows through the copper tube of evaporator, where water contacts its outer surface and becomes cool. Then the cooled water reaches to AMU. At the end, the refrigerant is delivered to the compressor through suction tube. Thus, the whole cycle is repeated perpetually.

B. BASIC OPERATION OF AMU ALONG WITH DEHUMIDIFIER

The connection between AMU and dehumidifier is illustrated in Fig. 10. Stainless steel pipes are used to create the network between cooling coils of AMU and the evaporator of chiller. Moreover, a cooled water pump is placed between them. The underlying AMU consists of cooling coil, supply fan motor, mixing box, and filtering unit. The backup water tank (BWT) ensures the uninterruptible water supply. With the help of chilled water pump, the cooled water produced by chiller flows through the SCWP and RCWP. The water entering into the cooling coil is called supply chilled water and water leaving the cooling coil is called return chilled

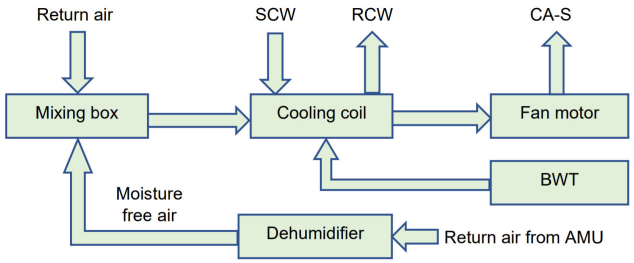

FIGURE 10. Connection between the dehumidifier and AMU.

water. During the operation of AMU, return air from the linear generator area passes through the cooling coil by supply fan motor. When the air mixes with cooling coil, its temperature decreases. Finally, this low temperature air flows around the proposed LG to make it cool.

Since the air contains water, it could be the main cause of rust formation on magnetic core of both translator and stator. For this reason, the cores could get affected by corrosion gradually and the generator would have poor efficacy. To avoid this problem, water is separated from air by applying a dehumidifier. The operating procedure of dehumidifier is depicted in Fig. 11.

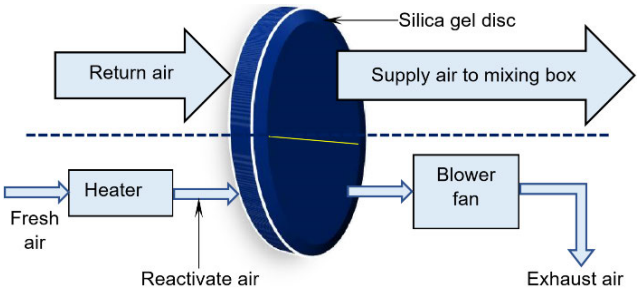

FIGURE 11. Simplified arrangement of the dehumidifier.

It consists of a disc driving induction motor, blower fan, electric heater, and a silica gel disc. The disc is rotated gradually with an induction motor. When return air coming from the LG area passes through the disc, the water is absorbed by disc materials. The dry air then reaches to the mix up box in AMU. At the same time, the water absorbing portion of the disc nearly saturates. For reactivation of disc, hot air (by heater) requires passing through saturated portion. When the blower fan starts, the natural air flows through the heater and gets heated. Further, the heated air passes through the saturated area of disc and absorbs the water. Finally, the air is exhausted to atmosphere. This procedure is also performed continuously.

The water free air is supplied to the mixing box in AMU which delivers the treated air to the surrounding area of linear generator by its regular working principle.

VI. SIMULATION RESULTS

At first, a DDLG is designed with the built-in computer aided system in the ANSYS/Maxwell. The design incorporates standard PM (N30H NdFeB), conventional magnetic core, X-4 copper wire and 4Ω load resistance. Power rating of the DDLG is 700kW for 1m/s velocity of the translator. Further, the same design is analyzed for copper wires having different cross-sectional sizes such as X-5, X-3, and X-2. To obtain better result, fine mesh setup is selected as shown in Fig. 12. As three-dimensional finite element analysis is performed, each of the element is mathematically represented by tetrahedra. Most of the elements exist around the pole faces. Moreover, with the aid of finite element analysis, the electrical and magnetic properties are analyzed.

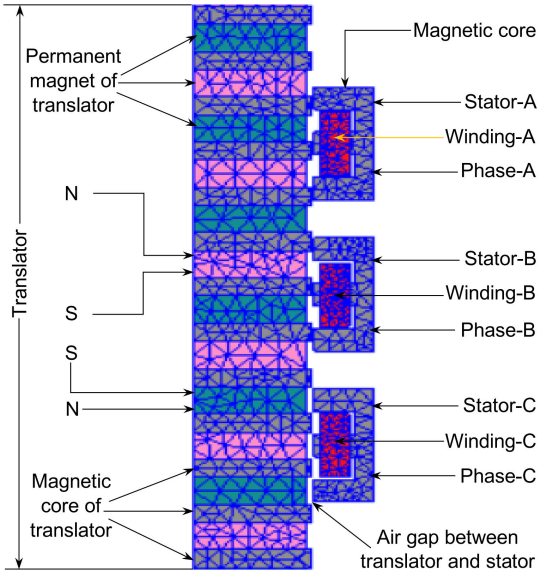

FIGURE 12. Mesh plot of the proposed linear generator.

The voltage waveforms for different conductor sizes are illustrated in Fig. 13. The rms value of voltages are 0.84kV, 1.23kV, 1.36kV, and 1.37kV for X-5, X-4, X-3, and X-2, respectively. The maximum voltage at the output terminal is observed for the thinnest wire. Fig. 14. shows the current waveforms of DDLG having different size of copper conductors. The currents (rms) are measured 231A, 291A, 316A, and 281A for X-5, X-4, X-3, and X-2 conductors, respectively. Hence, the DDLG with X-3 copper wire flows the maximum current than the others. Generated powers of the DDLG for using different wires are depicted in Fig. 15.

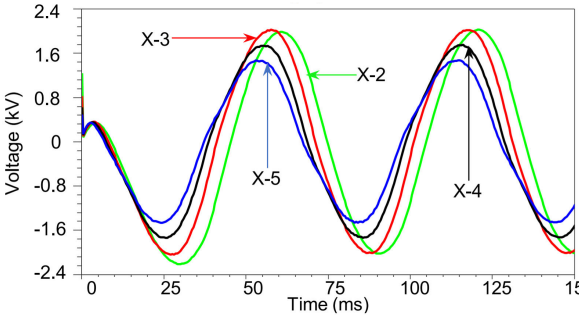

FIGURE 13. Induced voltage waveforms of the DDLG for different conductor size.

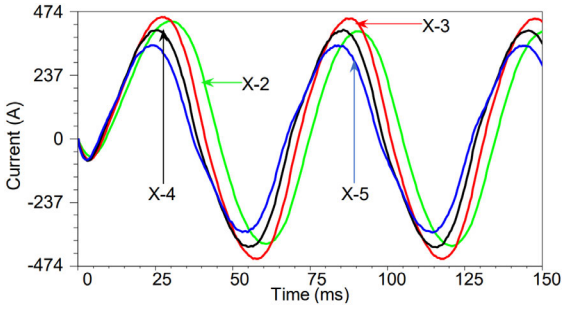

FIGURE 14. Load current waveforms of the DDLG for different conductor size.

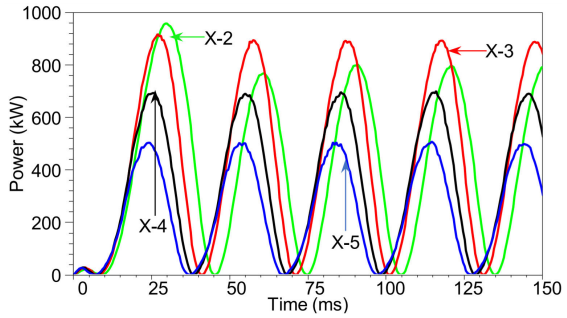

FIGURE 15. Generated power of the DDLG for different conductor sizes.

Even though the thinnest wire delivers the maximum power in the beginning, it reduces in its subsequent cycles. However, the power performance prevails for X-3 wire. The rms output powers are found 250kW, 350kW, 446kW, and 400kW for X-5, X-4, X-3, and X-2 conductors, respectively. The peak value of voltage, current, and power are tabulated in Table 3, where the DDLG with X-3 copper wire outperforms the others. Since, copper loss depends on the internal resistance of winding and load, performance of the X-3 winding based DDLG is observed for different load conditions. In this analysis, the load resistances are varied form 1–5Ω. The resistance with the value of 1Ω, 2Ω, 3Ω, 3.6Ω, 4Ω, and 5Ω are denoted by R_l-1, R_l-2, R_l-3, R_l-3.6, R_l-4, and R_l-5, respectively.

TABLE 3. Power, current, and voltage of the DDLG for different conductors.

Cross-sectional area (mm^2)	Power (kW)	Current (A)	Voltage (kV)
2	800	398.4	2.008
3	892	449	1.99
4	700	411.1	1.74
5	500	325.7	1.45

Output voltage and power waveforms are plotted in Figs. 16 and 17, respectively. The maximum voltage is found for 5Ω load whereas maximum power is found for 3Ω load. The generated output power, voltage, and current for various loads are tabulated in Table 4. The peak values of generated voltage, power, and load current for different loads are depicted in Fig. 18. From the results it is observed that,

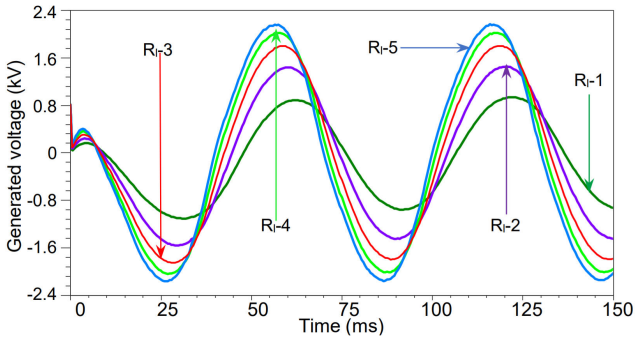

FIGURE 16. Generated output power of the DDLG at X-3 conductor.

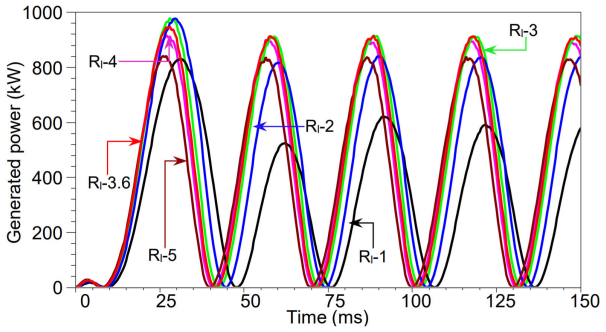

FIGURE 17. Generated output power of the DDLG at X-3 conductor.

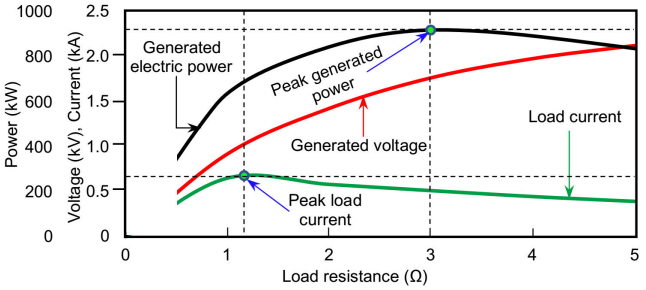

FIGURE 18. Generated power, voltage, and load current for different load resistance for X-3 conductor.

TABLE 4. Power, current, and voltage of the DDLG for X-3 Conductor.

Load (Ω)	Voltage (kV)	Current (A)	Power (kW)
1	0.92	654.5	625
2	1.43	585	840
3	1.78	515.4	912
3.6	1.92	471.1	911
4	1.99	449	892
5	2.13	395.3	835

for high load current, generated voltage is low and vice-versa. The maximum generated power is 912kW for the load resistance of 3Ω.

The power output (at the load) and copper loss are presented in Fig. 19 for different loads. The operating point is obtained for X-3 copper wire with 3.6Ω load resistance. The maximum copper loss and power are indicated with dots.

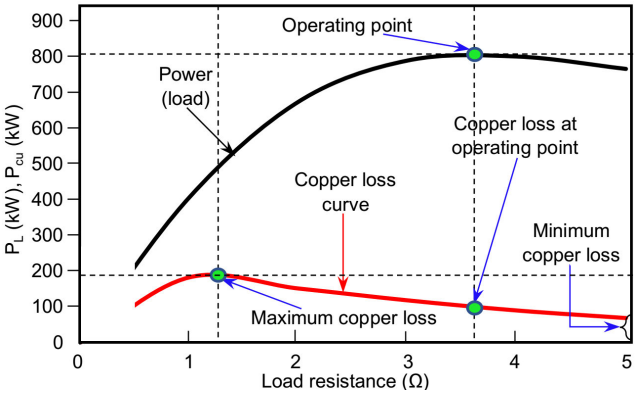

FIGURE 19. Load profile of the DDLG for X-3 conductor.

For 3.6Ω load resistance, approximately 810kW of power is delivered to the load, which is the highest power. On the other hand, 790kW is found for 3Ω. The maximum copper loss is 183kW which is also indicated in Fig. 19.

The high grade NdFeB permanent magnet, N45 is applied to the winding optimized DDLG to obtain even more power. In this case, the DDLG is named advanced DDLG (hereafter) and its power waveform is shown in Fig. 20. The rms value of the generated voltage and power are 1.36kV and 456kW, respectively. The comparison in magnetic flux linkage between the optimized and advanced DDLG (with N45) is shown in Fig. 21. It is found that the advanced one has better flux linkage than the other. The load currents of the DDLG are plotted in Fig. 22 where 474A and 506A currents are found for the optimized and the advanced DDLG, respectively.

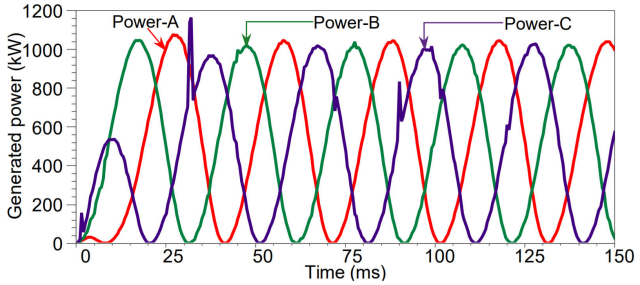

FIGURE 20. Output power of the advanced DDLG.

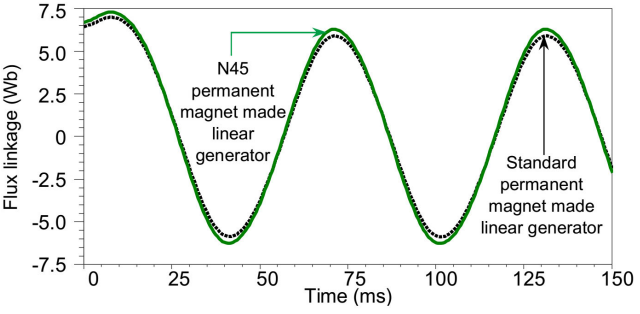

FIGURE 21. Plot of magnetic flux linkages of the optimized and advanced DDLG.

Voltage comparison between the two DDLGs is depicted in Fig. 23. The advanced DDLG generates more voltage than the other. Fig. 24 shows the generated output power of both the DDLGs where the advanced DDLG generates more output power than the other. A comparison between these two DDLGs is illustrated in Table 5.

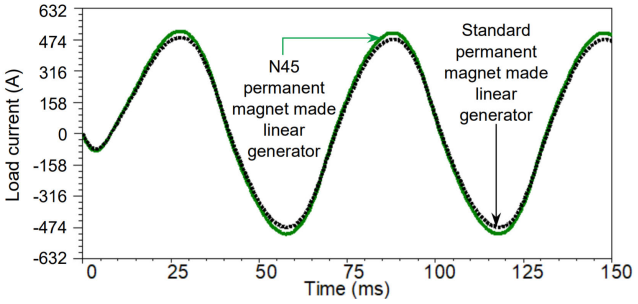

FIGURE 22. Load currents of the optimized and advanced DDLG.

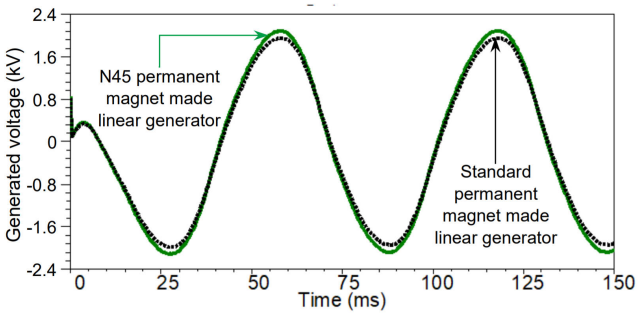

FIGURE 23. Induced voltages of the optimized and advanced DDLG.

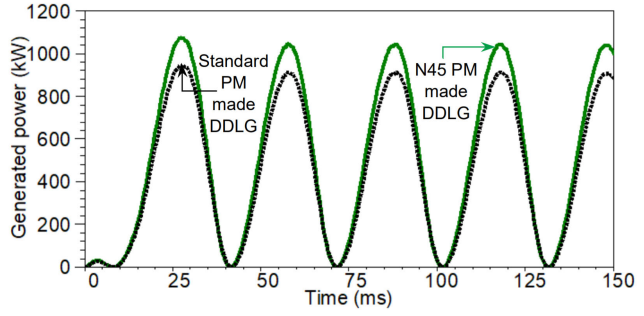

FIGURE 24. Generated output powers of the optimized and advanced DDLG.

TABLE 5. Comparison between the two DDLGs.

Output parameters	Optimized DDLG (Peak)	Advanced DDLG (Peak)
Generated voltage (kV)	1.93	2.05
Load current (A)	471	506
Generated power (kW)	911	1043
Power across load (kW)	804	922

The translator is made of magnetic core with permanent magnet and it is found from Fig. 6 that the remanence magnetism and coercivity of PM depends on operating

TABLE 6. Comparison among all DDLGs.

DDLG	Induced voltage (kV)	Current (A)	Generated power (kW)	Load power (kW)
Conventional DDLG	1.74	411	700	676
Optimized DDLG	1.93	471	911	804
Advanced DDLG	2.06	506	1043	922
Enhanced DDLG	2.30	569	1293	1166

temperature. As the magnetic remanence is low at high temperature, the DDLG cannot generate sufficient output power. To produce adequate output power, the advanced DDLG should be operated at the low temperature. Therefore, a cooling system is incorporated with it. Hereafter in this article, it is called enhanced DDLG.

The peak output voltage of the advanced and enhanced DDLG are compared in Fig. 25. The enhanced DDLG generates 2.3kV whereas the advanced one generates 2.05kV. Load current of the enhanced DDLG increases beyond the advanced one as shown in Fig. 26. Comparison of generated power between the two generators is depicted in Fig. 27. It is found that, the enhanced DDLG (that includes cooling system) generates 6.46% higher output power than the other. The output parameters of the conventional, optimized, advanced, and enhanced DDLGs are shown in Table 6. Fig. 28 shows the magnetic flux density (B) and field intensity (H) of the optimized DDLG. B and H are also analyzed to prevent demagnetization of the PMs. With the rainbow spectrum, the values of B and H are observed. The minimum value of B is found in the copper winding.

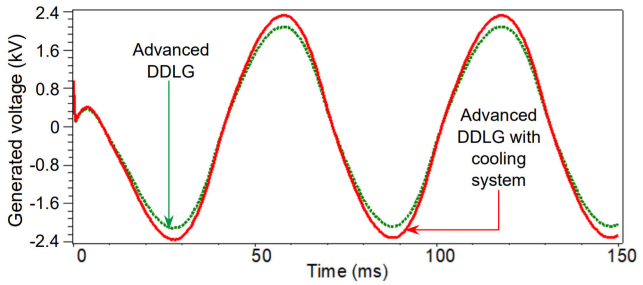

FIGURE 25. Comparison the voltage between the advanced and enhanced DDLGs (with cooling system).

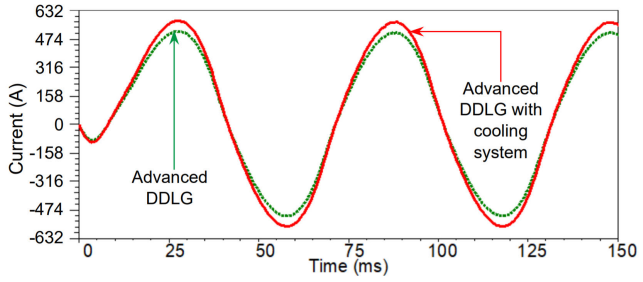

FIGURE 26. Comparison of the current waveforms between the advanced and enhanced DDLGs.

Magnetic flux density of the stators and their front faces are shown in Figs. 29 and 30. The analysis is required for both

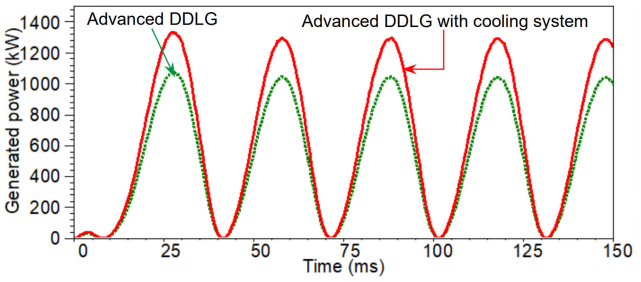

FIGURE 27. Comparison of the power between the advanced and enhanced DDLGs.

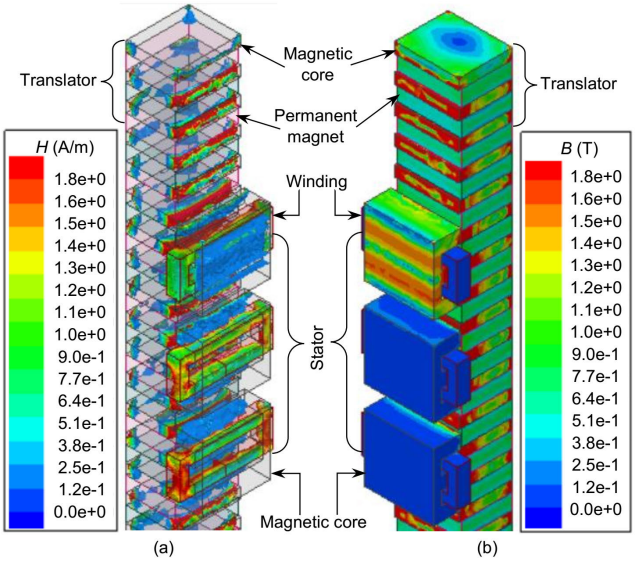

FIGURE 28. Analysis of magnetic property of the proposed enhanced DDLG.

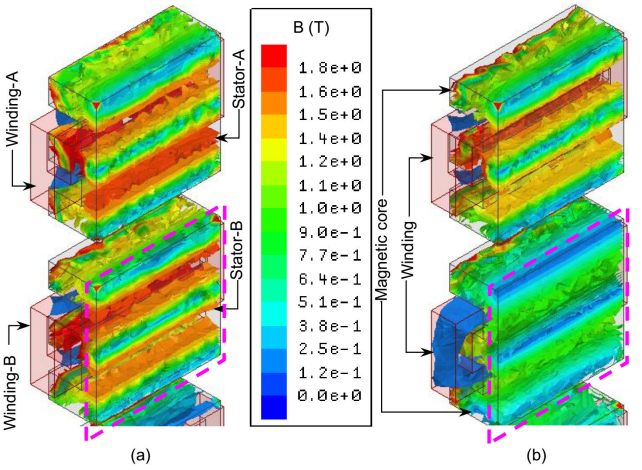

FIGURE 29. Magnetic flux density of the stator at: (a) the starting condition (t = 0ms) (b) the running condition (t = 100ms).

the starting and running condition of the DDLG to observe whether there is any magnetic saturation. From the analysis, it is found that the flux density in the stator almost saturates at standstill condition or at the starting condition. But in running condition, the flux density minimizes because of the armature

reaction. The major difference of flux density is identified in the dashed rectangles. The flux density varies over time in both the stators and their front faces. The highest flux density is found on the stator's front faces as shown in Fig. 30.

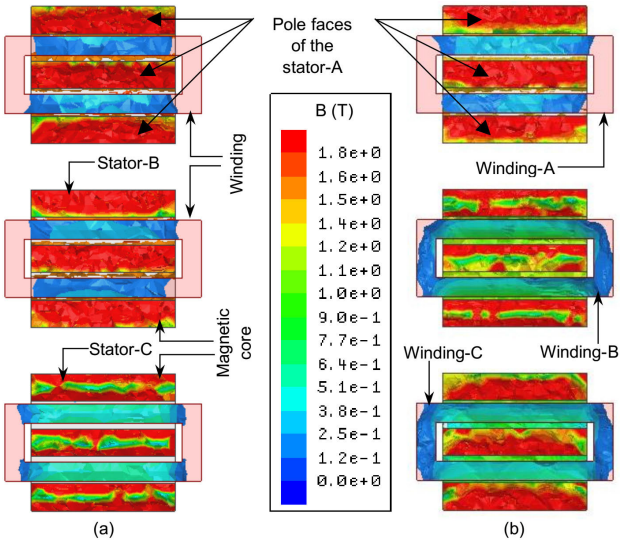

FIGURE 30. Distribution of magnetic flux density of the stator pole faces at: (a) the starting condition (t = 0ms) (b) the running condition (t = 100ms).

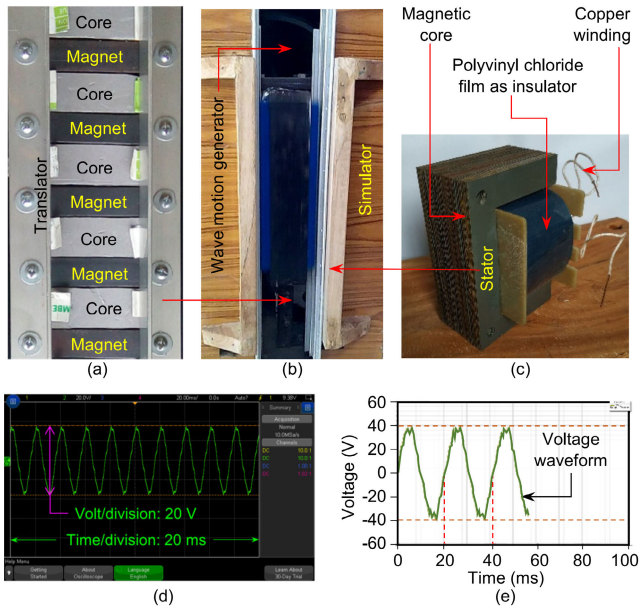

FIGURE 31. Construction of the prototype: (a) translator (b) simulator (c) stator (d) experimental result, and (e) simulation result.

The small-scale prototype of the proposed linear generator is constructed and presented in Fig. 31. It consists of a translator, simulator, and stator. The simulator creates a physical translational motion that moves the translator vertically with respect to the stator. The experimental and simulation results of the terminal voltage are shown in Figs. 31(d) and 31(e), respectively. A little variation is observed in the voltage waveforms. The design and working principle of the proposed DDLG (Fig. 4) and the small-scale prototype as shown in Figs. 31(a)–31(c) are similar. To compare the output voltage, another simulation result with the parameters of the prototype is presented in Fig. 31(e). The cooling system is not considered in the prototype.

The core loss curve of the magnetic material is plotted in Fig. 32. The amount of total core loss is found approximately 7kW after one cycle operation period. Because, the simulation software takes one cycle time to calculate the value properly.

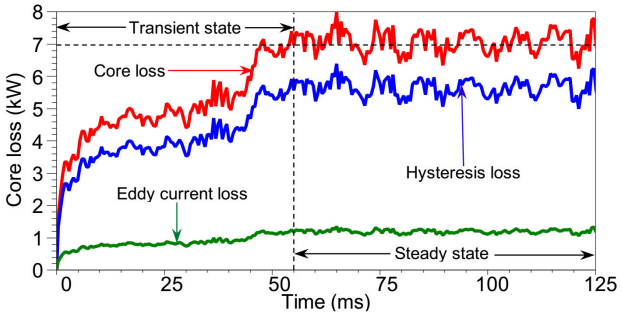

FIGURE 32. Core loss curve of the proposed DDLG.

The proposed winding topology also minimizes the material cost per unit generation. Considering the total material cost of the DDLG, C_t, the per unit (kW) cost becomes C_t /676 or 0.00148 C_t. Application of the proposed- optimized, advanced, and enhanced DDLG, per unit (kW) cost would become C_t/804, C_t/922, and C_t/1166, respectively. The calculation of material minimization cost is summarized in Table 7.

TABLE 7. Minimization of material Cost/kW of all the proposed DDLGs.

DDLG	Material cost/kW	Material cost minimization/kW (in each step)	Material cost minimization/kW (w.r.t conventional)
Conventional DDLG	0.00148 C_t	0%	0%
Optimized DDLG	0.00124 C_t	16.22%	16.22%
Advanced DDLG	0.00108 C_t	12.90%	27.03%
Enhanced DDLG	0.00086 C_t	20.37%	41.89%

*w.r.t means with respect to

VII. CONCLUSION

This article proposes a new winding optimization method along with high graded magnetic material and cooling system. To test the performance of the proposed method, an LG is designed and simulated by using finite element method. Electrical and magnetic properties of the LG are observed. It is found that, the proposed optimized and enhanced DDLG produces the highest output. Magnetic properties are also analyzed along with winding optimization. As the core loss is almost fixed for a specific frequency of operation, copper loss is focused because it depends on the load condition. Furthermore, electrical power is again increased by using

high graded N45 NdFeB. During operation, temperature of the LG often rises because of various losses. The rising temperature needs to be minimized as it noticeably decreases the remanence of either standard or high graded PMs. For this reason, a cooling system is proposed and discussed along with winding optimization. From the cost analysis, it is also found that the proposed DDLG greatly minimizes the material cost per unit power (kW) generation. The total core loss is found only 0.6% of its maximum load power. The volumetric electrical power density of the enhanced DDLG is increased by 41.89%. It is expected that the proposed winding optimization method can be used in designing other linear generators to improve their performances.

APPENDIX
NOMENCLATURE

ACRONYM

AMU	Air management unit
BWT	Backup water tank
DDLG	Direct drive linear generator
DHF	Dehumidifier
$Fe_{16}N_2$	Iron nitride
LG	Linear generator
NdFeB	Neodymium iron boron
PM	Permanent magnet
RCWP	Return chilled water pipe
SCWP	Supply chilled water pipe

SYMBOL

A	Cross-sectional area (mm^2)
B	Magnetic flux density (T)
B_m	Maximum flux density (T)
c	Constant that depends on properties of the magnetic material
E_F	Voltage of equivalent field (V)
E'_f	Transient excitation voltage (V)
E_f	Excitation voltage (V)
E_i	Voltage across/behind X_d (V)
e	Induced voltage in stator (V)
f	Voltage frequency (Hz)
f_{do}	Voltage of d-axis without damper (V)
f_{qo}	Voltage in q-axis without damper (V)
g	Gravitational constant (9.81 ms^{-2})
H	Magnetic field intensity (A-m^{-1})
H_s	Height of stator (m)
H_t	Height of translator (m)
H_w	Height of wave (m)
I_a	Armature current (A)
I_d	Current in d axis (A)
I_q	Current in q axis (A)
L	Length of copper wire (m)
L_c	Core's length of translator (m)
L_m	PM's length of translator (m)
L_s	Winding's length of stator (m)
L_t	Length of translator (m)
M_e	Core loss components
m_a	Mass flowrate of air (kg-s^{-1})
m_{ar}	Nominal mass flowrate of air entering the cooling tower (kg-s^{-1})
m_{te}	Mass flowrate of water entering the tower (kg-s^{-1})
m_{tl}	Mass flowrate of water leaving the tower (kg-s^{-1})
N	Number of turns
P	Fan power (W)
P_{ad}	Excess loss (W)
P_c	Total core loss (W)
P_{cu}	Copper loss (W)
P_e	Eddy current loss (W)
P_h	Hysteresis loss (W)
P_r	Rated power of the fan (W)
P_0	Output power (W)
P_w	Wave power (W)
R	Resistance (Ω)
r_a	Resistance of stator winding (Ω)
S_a	No load rms stator voltage of phase-A (V)
T	Time period of wave (s)
t	Time (s)
t_c	Core's thickness of translator (m)
t_m	PM's thickness of translator (m)
V_d	Voltage in d axis (V)
V_q	Voltage in q axis (V)
V_t	Terminal voltage (V)
W_m	PM's width of translator (m)
W_s	Winding's width of stator (m)
W_t	Width of translator (m)
X_d	Synchronous reactance in d axis (Ω)
X'_d	Transient reactance in d axis (Ω)
X_q	Synchronous reactance in q axis (Ω)
δ	Force angle (°)
θ	Power factor angle (°)
ρ	Specific resistivity (Ω-m^{-1})
ρ_w	Mass density of sea water (1025 kg-m^{-3})
φ	Magnetic flux (Wb)
ω_{tl}	Moisture content of air leaving the tower (kg-kg^{-1} dry air)
ω_{te}	Moisture content of air entering the tower (kg-kg^{-1} dry air)

REFERENCES

[1] S. Molla, O. Farrok, M. R. Islam, and K. M. Muttaqi, "Analysis and design of a high performance linear generator with high grade magnetic cores and high temperature superconducting coils for oceanic wave energy conversion," *IEEE Trans. Appl. Supercond.*, vol. 29, no. 2, pp. 1–5, Mar. 2019.
[2] H. Huang, "Ferroelectric photovoltaics," *Nature Photon.*, vol. 4, pp. 134–135, Mar. 2010.
[3] R. Basak, G. Bhuvaneswari, and R. R. Pillai, "Low-voltage ride-through of a synchronous generator-based variable speed grid-interfaced wind energy conversion system," *IEEE Trans. Ind. Appl.*, vol. 56, no. 1, pp. 752–762, Jan. 2020.
[4] C. Carounagarane, T. R. Chelliah, and D. Khare, "Analysis on thermal behavior of large hydrogenerators operating with continuous overloads," *IEEE Trans. Ind. Appl.*, vol. 56, no. 2, pp. 1293–1305, Mar. 2020.
[5] M. O. Hamdan, "Tapping to geothermal energy through a high performance Earth-to-water heat exchanger design," in *Proc. 5th Int. Conf. Renew. Energy, Gener. Appl. (ICREGA)*, Feb. 2018, pp. 207–210.

[6] S. Chandrasekaran and B. Raghavi, "Design, development and experimentation of deep ocean wave energy converter system," *Energy Procedia*, vol. 79, pp. 634–640, Nov. 2015.

[7] O. Farrok, K. Ahmed, A. D. Tahlil, M. M. Farah, M. R. Kiran, and M. R. Islam, "Electrical power generation from the oceanic wave for sustainable advancement in renewable energy technologies," *Sustainability*, vol. 12, no. 6, pp. 1–23, Mar. 2020.

[8] M. A. Kowser, M. T. Islam, M. A. Chowdhury, T. B. Chakma, M. G. Uddin, and M. Z. R. Chowdhury, "Performance measurement of a newly proposed ocean wave energy conversion system," in *Proc. 5th Int. Conf. Environ. Aspects Bangladesh*, Dhaka, Bangladesh, 2014, pp. 74–76.

[9] S. Lindroth and M. Leijon, "Offshore wave power measurements—A review," *Renew. Sustain. Energy Rev.*, vol. 15, no. 9, pp. 4274–4285, Dec. 2011.

[10] I. A. Ivanova, O. Agren, H. Bernhoff, and M. Leijon, "Simulation of wave-energy converter with octagonal linear generator," *IEEE J. Ocean. Eng.*, vol. 30, no. 3, pp. 619–629, Jul. 2005.

[11] S. G. Siegel, "Numerical benchmarking study of a cycloidal wave energy converter," *Renew. Energy*, vol. 134, pp. 390–405, Apr. 2019.

[12] O. Farrok, M. R. Islam, K. M. Muttaqi, D. Sutanto, and J. Zhu, "Design and optimization of a novel dual-port linear generator for oceanic wave energy conversion," *IEEE Trans. Ind. Electron.*, vol. 67, no. 5, pp. 3409–3418, May 2020.

[13] L. Li, Z. Yuan, and Y. Gao, "Maximization of energy absorption for a wave energy converter using the deep machine learning," *Energy*, vol. 165, pp. 340–349, Dec. 2018.

[14] H. M. Hasanien, "Transient stability augmentation of a wave energy conversion system using a water cycle algorithm-based multiobjective optimal control strategy," *IEEE Trans. Ind. Informat.*, vol. 15, no. 6, pp. 3411–3419, Jun. 2019.

[15] H. M. Hasanien, "Gravitational search algorithm-based optimal control of archimedes wave swing-based wave energy conversion system supplying a DC microgrid under uncertain dynamics," *IET Renew. Power Gener.*, vol. 11, no. 6, pp. 763–770, May 2017.

[16] L. Huang, J. Liu, H. Yu, R. Qu, H. Chen, and H. Fang, "Winding configuration and performance investigations of a tubular superconducting flux-switching linear generator," *IEEE Trans. Appl. Supercond.*, vol. 25, no. 3, pp. 1–5, Jun. 2015.

[17] S. Molla and O. Farrok, "Vitroperm 500F and supermendur ferromagnetic cores used in a linear generator for oceanic wave energy conversion," in *Proc. Int. Conf. Robot., Elect. Signal Process. Techn. (ICREST)*, Dhaka, Bangladesh, Jan. 2019, pp. 602–605.

[18] S. Molla, O. Farrok, M. R. Islam, and K. M. Muttaqi, "Application of iron nitride compound as alternative permanent magnet for designing linear generators to harvest oceanic wave energy," *IET Electr. Power Appl.*, vol. 14, no. 5, pp. 762–770, May 2020.

[19] S. Molla and O. Farrok, "Use of high flux density ferromagnetic cores in linear generators for oceanic wave energy conversion," in *Proc. Int. Conf. Electr., Comput. Commun. Eng. (ECCE)*, Coxbazar, Bangladesh, Feb. 2019, pp. 1–5.

[20] B. Ekergård and M. Leijon, "Longitudinal end effects in a linear wave power generator," *Energies*, vol. 13, no. 2, Jan. 2020, Art. no. 327.

[21] O. Farrok, M. R. Islam, Y. Guo, J. Zhu, and W. Xu, "A novel design procedure for designing linear generators," *IEEE Trans. Ind. Electron.*, vol. 65, no. 2, pp. 1846–1854, Feb. 2018.

[22] L. Huang, H. Yu, M. Hu, J. Zhao, and Z. Cheng, "A novel flux-switching permanent-magnet linear generator for wave energy extraction application," *IEEE Trans. Magn.*, vol. 47, no. 5, pp. 1034–1037, May 2011.

[23] R. Guanche, V. Gómez, C. Vidal, and I. Eguinoa, "Numerical analysis and performance optimization of a submerged wave energy point absorber," *Ocean Eng.*, vol. 59, pp. 214–230, Feb. 2013.

[24] E. Abraham and E. C. Kerrigan, "Optimal active control and optimization of a wave energy converter," *IEEE Trans. Sustain. Energy*, vol. 4, no. 2, pp. 324–332, Apr. 2013.

[25] O. Farrok, M. R. Islam, M. R. I. Sheikh, and W. Xu, "A new optimization methodology of the linear generator for wave energy conversion systems," in *Proc. IEEE Int. Conf. Ind. Technol. (ICIT)*, Taipei, Taiwan, Mar. 2016, pp. 1412–1417.

[26] F. W. Yu and K. T. Chan, "Optimization of water-cooled chiller system with load-based speed control," *Appl. Energy*, vol. 85, no. 10, pp. 931–950, Oct. 2008.

SELIM MOLLA (Member, IEEE) received the B.Sc. degree from the Department of Electrical and Electronic Engineering (EEE), World University of Bangladesh, and the M.Sc. degree from the Department of EEE, Ahsanullah University of Science and Technology (AUST).

He is currently serving with the Engineering Department of a state owned pharmaceutical named Essential Drugs Company Ltd., under the Ministry of Health and Family Welfare, Government of the People's Republic of Bangladesh. Besides his professional job, he engaged himself in research activities under the supervision of Dr. Omar Farrok, an Associate Professor with the Department of EEE, AUST. He has authored more than seven technical papers in international journals and conference proceedings. His research interests include renewable energy systems, oceanic wave energy converters, electrical machines and drives, magnetic properties of materials, electromagnetics, and power electronics. He achieved the Best Presentation Award in ASEMD-2018, Tianjin, China, in 2018.

OMAR FARROK (Member, IEEE) received the Ph.D. degree from the Department of Electrical and Electronic Engineering (EEE), Rajshahi University of Engineering and Technology (RUET), Rajshahi, Bangladesh, in 2016.

Since 2016, he has been a Distinct Associate Professor with the Department of EEE, Ahsanullah University of Science and Technology (AUST), Dhaka, Bangladesh. He has authored or coauthored more than 60 technical papers in the international journals and conference proceedings, including ten IEEE TRANSACTIONS/Journal articles. His research interests include permanent magnet machines, linear electrical generator, magnetic material, renewable energy systems, oceanic wave energy converter, electrical machine and drive, electromagnetics, and power electronics. He is a Life Fellow of the Institution of Engineers, Bangladesh (IEB). He received Four Best Paper Awards from the IEEE ICEMS, Sydney, NSW, Australia, in 2017; ASEMD, Tianjin, China, in 2018; ICEMS, Harbin, China, in 2019; and PEEIACON, Dhaka, in 2019. He is elected as the Chair, the Co-Chair, and nominated as a member of several technical committees formed by the Bangladesh Government under the Ministry of Industries and others. He was registered with the Board of Bangladesh Professional Engineers Registration Board (BPERB), as a Professional Engineer (P.Eng.), in 2017.

ABIDUR RAHMAN received the B.Sc. and M.Sc. degrees in electrical and electronic engineering (EEE) from the Ahsanullah University of Science and Technology (AUST), Dhaka, Bangladesh, in 2016 and 2020, respectively.

He has been a Lecturer with the Department of EEE, AUST, since 2019. He also held the position of a Lecturer with the Northern University Bangladesh, Dhaka, from 2016 to 2018. His research interests include smart grid, renewable energy sources, and electric machines. He was awarded with the Dean's List of Honor for academic excellence.

MD. SAMIUL BASHIR received the B.Sc. and M.Sc. degrees from the Department of Electrical and Electronic Engineering (EEE), Ahsanullah University of Science and Technology.

He has been serving as an Electrical Engineer with Active Fine Chemicals Ltd., since January 2010, where he is currently working as a Research Assistant. Besides his professional job, he engaged himself in research activities under the supervision of Dr. Omar Farrok, an Associate Professor with the Department of EEE, AUST. He has authored more than four technical papers in international conference proceedings. His research interests include renewable energy systems, oceanic wave energy converters, electrical machines and drives, magnetic properties of materials, electromagnetics, and power electronics.

MD. RABIUL ISLAM (Senior Member, IEEE) received the Ph.D. degree in electrical engineering from the University of Technology Sydney (UTS), Sydney, Australia, in 2014.

He was appointed a Lecturer with RUET, in 2005, where he was promoted to a Full Professor, in 2017. In early 2018, he joined at the School of Electrical, Computer, and Telecommunications Engineering (SECTE), University of Wollongong (UOW), Wollongong, Australia. His research interests include power electronic converters, renewable energy technologies, power quality, electrical machines, electric vehicles, and smart grid. He has authored or coauthored more than 170 papers, including 49 IEEE Transactions/IEEE Journal articles. He has written or edited technical books published by Springer. He has received several funding from Government and Industries, including the Australian Government ARC Discovery Project 2020 titled "A Next Generation Smart Solid-State Transformer for Power Grid Applications." He has served as a Guest Editor for the IEEE Transactions on Energy Conversion, the IEEE Transactions on Applied Superconductivity, and *IET Electric Power Applications*. He has been serving as an Editor for the IEEE Transactions on Energy Conversion and the IEEE Power Engineering Letters, and an Associate Editor for IEEE Access.

ABBAS Z. KOUZANI (Member, IEEE) received the B.Sc. degree in computer engineering from the Sharif University of Technology, Iran, the M.Eng.Sc. degree in electrical and electronic engineering from the University of Adelaide, Australia, and the Ph.D. degree in electrical and electronic engineering from Flinders University, Australia. He was a Lecturer with the School of Engineering, Deakin University, Australia, and then a Senior Lecturer with the School of Electrical Engineering and Computer Science, University of Newcastle, Australia. He is currently a Professor with the School of Engineering, Deakin University, where he is also the Director of the Advanced Integrated Microsystems (AIM) Research Group. He provides research leadership in embedded, connected, and low-power devices, circuits, and instruments that incorporate sensing, actuation, control, wireless transmission, networking and the IoT, data acquisition/storage/analysis, AI, energy harvesting, power management, and fabrication for tackling research questions relating to a variety of disciplines, including healthcare, ecology, mining, infrastructure, automotive, manufacturing, energy, utilities, and agriculture. He has produced over 370 publications, including one book, 17 book chapters, 180 journal articles, and 181 fully refereed conference papers. He has three patents and two pending patents. He has been involved in over $15 million research grants, and has managed projects and delivered research solutions to over 25 Australian and International companies. He received several awards, including the Outstanding Contribution to Scholarly Publication Award from the School of Engineering, Deakin University, in 2019. He has supervised 24 research fellows/assistants, and produced 28 Ph.D. and six Masters by Research completions. He is also involved in supervision of 12 Ph.D. students.

M. A. PARVEZ MAHMUD received the B.Sc. degree in electrical and electronic engineering and the Master of Engineering degree in mechatronics engineering. After the successful completion of his Ph.D. degree with multiple awards, he has worked as a Postdoctoral Research Associate and an Academician with the School of Engineering, Macquarie University, Sydney. He is currently an Alfred Deakin Postdoctoral Research Fellow with Deakin University. He has worked as a Lecturer with the World University of Bangladesh (WUB), for more than two years, and a Researcher with the Korea Institute of Machinery and Materials (KIMM), for about three years. His research interests include energy sustainability/harvesting, sensors, and electric microgrid control and management.